Accepted Manuscript

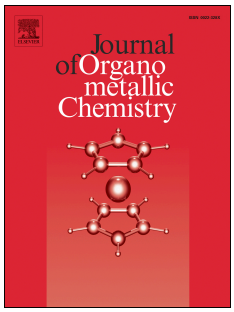

Neutral and cationic half-sandwich arene ruthenium, Cp*Rh and Cp*Ir oximato and oxime complexes: Synthesis, structural, DFT and biological studies

Sanjay Adhikari, Narasinga Rao Palepu, Dipankar Sutradhar, Samantha L. Shepherd, Roger M. Phillips, Werner Kaminsky, Asit K. Chandra, Mohan Rao Kollipara

PII: S0022-328X(16)30325-4

DOI: 10.1016/j.jorganchem.2016.08.004

Reference: JOM 19583

To appear in: *Journal of Organometallic Chemistry*

Received Date: 19 June 2016

Revised Date: 21 July 2016

Accepted Date: 2 August 2016

Please cite this article as: S. Adhikari, N.R. Palepu, D. Sutradhar, S.L. Shepherd, R.M. Phillips, W. Kaminsky, A.K. Chandra, M.R. Kollipara, Neutral and cationic half-sandwich arene ruthenium, Cp*Rh and Cp*Ir oximato and oxime complexes: Synthesis, structural, DFT and biological studies, *Journal of Organometallic Chemistry* (2016), doi: 10.1016/j.jorganchem.2016.08.004.

Neutral and cationic half-sandwich arene ruthenium, Cp*Rh and Cp*Ir oximato and oxime complexes: Synthesis, structural, DFT and biological studies.

Sanjay Adhikari[a], Narasinga Rao Palepu[a], Dipankar Sutradhar[a], Samantha L Shepherd[b], Roger M Phillips[b], Werner Kaminsky[c], Asit K. Chandra[a], Mohan Rao Kollipara[a*]

[a]Centre for Advanced Studies in Chemistry, North-Eastern Hill University, Shillong 793022, India. E-mail: mohanrao59@gmail.com

Telephone Number: +91 364 2722620

Fax Number: +91 364 2550076

[b]Department of Pharmacy, School of Applied Sciences, University of Huddersfield, Huddersfield HD1 3DH, UK

[c]Department of Chemistry, University of Washington, Seattle, WA 98195, USA

Graphical Abstract

Reaction of strongly electron withdrawing cyano substituted pyridyl oxime with metal precursor afforded the neutral oximato metal complexes due to the deprotonation of the oxime hydrogen whereas reaction of weakly electron donating substituted phenyl and methyl oximes yielded cationic oxime complexes. The iridium complexes were found to be more active against MIAPaCa-2 cancer cell line.

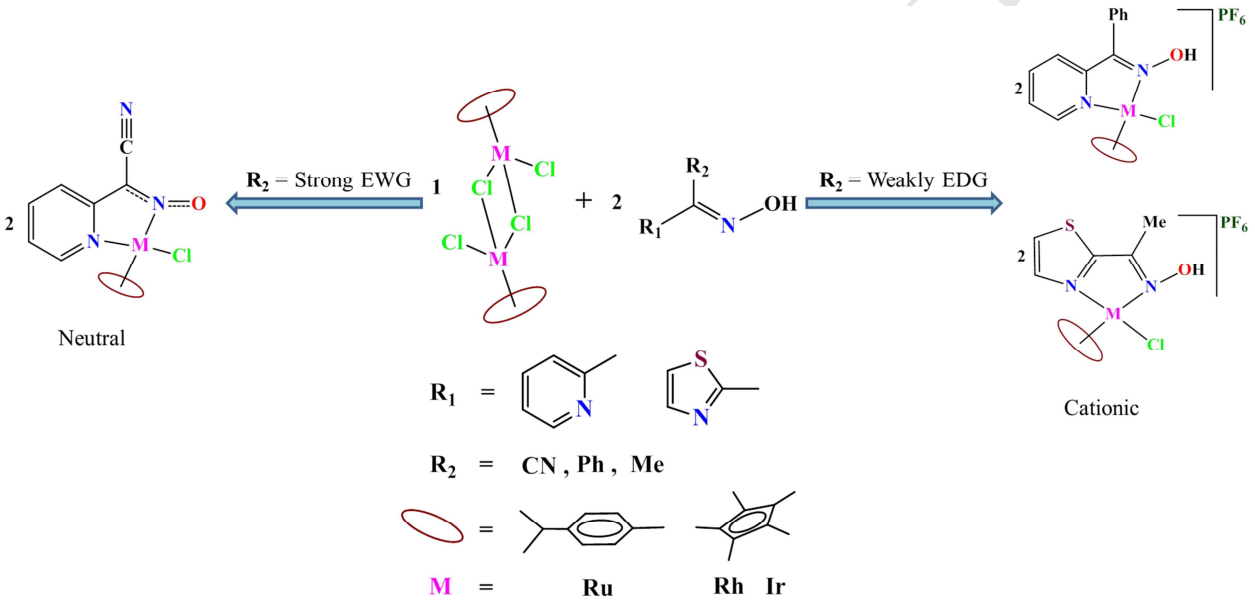

Abstract

The reaction of $[(p\text{-cymene})RuCl_2]_2$ and $[Cp^*MCl_2]_2$ (M = Rh/Ir) with chelating ligand 2-pyridyl cyanoxime {pyC(CN)NOH} leads to the formation of neutral oximato complexes having the general formula [(arene)M{pyC(CN)NO}Cl] {arene = *p*-cymene, M = Ru, (**1**); Cp*, M = Rh (**2**); Cp*, M = Ir (**3**)}. Whereas the reaction of 2-pyridyl phenyloxime {pyC(Ph)NOH} and 2-thiazolyl methyloxime {tzC(Me)NOH} with precursor compounds afforded the cationic oxime complexes bearing formula $[(arene)M\{pyC(ph)NOH\}Cl]^+$ and $[(arene)M\{tzC(Me)NOH\}Cl]^+$ {arene = *p*-cymene M = Ru, (**4**), (**7**); Cp*, M = Rh (**5**), (**8**); Cp*, M = Ir (**6**), (**9**)}. The cationic complexes were isolated as their hexafluorophosphate salts. All these complexes were fully characterized by analytical, spectroscopic and X-ray diffraction studies. The molecular structures of the complexes revealed typical piano stool geometry around the metal center within which the ligand acts as a NN´ donor chelating ligand. The Chemo-sensitivity activities of the complexes evaluated against HT-29 (human colorectal cancer), and MIAPaCa-2 (human pancreatic cancer) cell line showed that the iridium-based complexes are much more potent than the ruthenium and rhodium analogues. Theoretical studies were carried out to have a deeper understanding about the charge distribution pattern and the various electronic transitions occurring in the complexes.

Keywords: Ruthenium, rhodium, iridium, oximes, cytotoxicity

1. Introduction

The study of half-sandwich arene ruthenium (arene = *p*-cymene and its derivatives) Cp*Rh and Cp*Ir complexes represents one of the most versatile subject in the field of organometallic chemistry because of their potential applications in various areas [1-6]. These complexes bearing the general formula $[(arene)(M)(L)X]^+$ (M = Ru, Rh and Ir, L is a chelating ligand and X is a halide) have been extensively studied as potential metal-based anticancer drugs [7-11]. The coordination sphere of the metal center in these half-sandwich complexes is stabilized by the arene moiety which protects the metal's oxidation state occupying three coordinating sites, the chelating ligand L which controls the reactivity through various interactions and the M-Cl bond which easily gets dissociated and produces the active site for the metal ion to target biomolecules [12, 13]. It is seen that the leaving group, the chelating ligand and the arene substituent strongly influence the biological and structure activity relationship of these complexes [14]. Sadler *et. al* carried out number of experiments with chelating N,N-, N,O- and O,O- ligands to study the SAR activity of cytotoxic ruthenium(II) complexes by increasing the size of the arene ring [15]. Also it has been proposed by various research groups that the cytotoxicity of half-sandwich metal complexes increases with increase in size of the arene substituent [16-18]. These complexes have also displayed their remarkable activity as catalyst in various organic transformation reactions such as hydrogenation, water oxidation and C-H activation [19-21]. In recent years many half-sandwich complexes with NN′ chelating nitrogen donor ligands have been accomplished in our laboratory [22].

Oxime ligands in particular have developed a keen interest in the field of coordination chemistry [23]. The oxime ligand can act as an ambidentate ligand and can coordinate with metal ions either through nitrogen or oxygen atoms [24]. Cyanoximes having the general formula

{HO-N=C(CN)-R}, where R is an electron withdrawing group represents an important class of biologically active compounds and transition metal complexes of cyanoximes have shown pronounced cytotoxicity and antimicrobial activity [25, 26]. The presence of the cyano group as a substituent close to the oxime fragment increases the acidity of the oxime several thousand times greater than that of common oximes [27]. The anions of 2-pyridyl oximes serve as a versatile ligand for preparation of complexes with unusual topologies exhibiting interesting magnetic properties [28]. Oximes have the capability to remain intact in the co-ordination sphere of the metal by undergoing O-H bond cleavage to afford oximate derivatives [29]. Despite having a rich diversified chemistry of metal oxime and oximato complexes, it is noteworthy that only a few half-sandwich platinum group metal oxime complexes have been reported to date [30, 31].

In our present work we report the synthesis of ruthenium, rhodium and iridium half-sandwich oximato and oxime complexes, their biological activity and theoretical studies. Ligands used in the present study are shown in Chart-1.

2 Experimental

2.1. Materials and methods

All reagents were purchased from commercial sources and used as received without further purification. $RuCl_3.nH_2O$, $RhCl_3.nH_2O$, $IrCl_3.nH_2O$ was purchased from Arora Matthey limited. 2-acetylthiazole and 2-benzoylpyridine were obtained from Aldrich, 2-pyridylacetonitrile was obtained from Alfa Aesar and hydroxylamine hydrochloride was obtained from himedia. The solvents were purified and dried according to standard procedures [32]. The starting precursor metal complexes $[(p\text{-cymene})RuCl_2]_2$ and $[Cp^*MCl_2]_2$ (M = Rh/Ir) were prepared according to the literature methods [33, 34]. The oxime ligands 2-pyridyl

cyanoxime, 2-pyridyl phenyloxime and 2-thiazolyl methyloxime were synthesized according to published procedures [29, 35 and 36]. Infrared spectra were recorded on a Perkin-Elmer 983 spectrophotometer by using KBr pellets in the range of 400-4000 cm^{-1}. ^1H NMR spectra were recorded on a Bruker Avance II 400 MHz spectrometer using DMSO-d_6 as solvents. Absorption spectra were recorded on a Perkin-Elmer Lambda 25 UV/Vis spectrophotometer in the range of 200-800 nm at room temperature in acetonitrile. Mass spectra were recorded using Q-Tof APCI-MS instrument (model HAB 273). Elemental analyses of the complexes were performed on a Perkin-Elmer 2400 CHN/S analyzer.

2.2. Structure determination by X-ray crystallography

Suitable single crystals of complexes (**1**), (**2**) and (**3**), were obtained by slow diffusion of hexane into acetone solution and crystals of complexes (**4**), (**5**), (**7**) and (**8**) were obtained by diffusing hexane into DCM solution. Single crystal X-ray diffraction data for the complexes were collected on an Oxford Diffraction Xcalibur Eos Gemini diffractometer at 293 K using graphite monochromated Mo-Kα radiation (λ = 0.71073 Å). The strategy for the data collection was evaluated using the CrysAlisPro CCD software. Crystal data were collected by standard ''phi–omega scan'' techniques and were scaled and reduced using CrysAlisPro RED software. The structures were solved by direct methods using SHELXS-97 and refined by full-matrix least squares with SHELXL-97 refining on F^2 [37, 38]. The positions of all the atoms were obtained by direct methods. Metal atoms in the complex were located from the E-maps and non-hydrogen atoms were refined anisotropically. The hydrogen atoms bound to the carbon were placed in geometrically constrained positions and refined with isotropic temperature factors, generally 1.2 U_{eq} of their parent atoms. Crystallographic and structure refinement parameters for the complexes are summarized in Table 1, and selected bond lengths and bond angles are presented

in Table 2. Figures 1-3 were drawn with ORTEP3 program whereas Figures S2-S6 was drawn by using MERCURY 3.6 program [39].

The crystal structure of complex (**5**) contains disordered hexane molecule, which has been removed by SQUEEZE method [40]. Crystal structure of complex (**6**) contains fourfold disordered solvent molecule, which has been refined and removed by SQUEEZE method. Crystal structure of complex (**8**) contains solvent molecule in their solved structure.

2.3. Biological studies

The complexes (**1**-**9**) were dissolved in DMSO at 100 mM and stored at -20 °C until required. The cytotoxicity of the complexes was studied against HT-29 (human colorectal cancer) and MIAPaCa-2 (human pancreatic cancer) cell line. Cells were seeded into 96 well plates at 1 x 10^3 cells per well and incubated at 37 $^{\circ}$C in a CO_2 enriched (5%), humidified atmosphere overnight to adhere. The cells were exposed to a range of drug concentrations in the range of 0-100 µM for four days before cell survival was determined using the MTT assay [41]. To each well MTT (0.5 mg/ml) in phosphate buffered saline was added and was further incubated at 37 $^{\circ}$C for 4 hours. The MTT was then removed from each well and the formazan crystals formed were dissolved in 150 µM DMSO and the absorbance of the resulting solution was recorded at 550 nm using an ELISA spectrophotometer. The percentage of cell inhibition was calculated by dividing the absorbance of treated cell by the control value absorbance (exposed to 0.1 % DMSO). The IC_{50} values were determined from plots of % survival against drug concentration. Each experiment was repeated three times and a mean value obtained and stated as IC_{50} (µM) ± SD.

2.4. Computational Methodology

The geometry optimization of all the complexes were done in the gas phase using the Density Functional Theory (DFT) based B3LYP method in conjugation with 6-31G** basis set for lighter atoms (H, C, N, O, Cl, S, P and F) and LANL2DZ [42, 43] basis set for heavier atoms (Ru, Rh and Ir). LANL2DZ is a widely used Effective Core Potential (ECP) basis set which considers the core electrons as chemically inactive and performs only on the valence electrons and thus reduces the computational cost. Harmonic frequency calculations were carried out at the same level to ensure that the geometries are minima at the potential energy surface (PES). Natural Bond Orbital (NBO) [44] analysis was carried out to get charges on individual atoms present in the complexes. Time dependent-Density Functional Theory (TD-DFT) [45] has been employed to evaluate the absorption spectra and the electronic transitions of the metal complexes. In order to incorporate the effect of the solvent around the molecule, the Polarizable Continuum Model (PCM) [46] was used in TD-DFT calculations. The composition of the molecular orbital analysis was carried out using the Chemissian software package [47]. All the electronic energy calculations were carried out using Gaussian 09 suite of program [48].

*2.5. General procedure for synthesis of neutral complexes (**1-3**)*

A mixture of starting metal precursor (0.1 mmol) and ligand 2-pyridyl cyanoxime, {pyC(CN)NOH} (0.2 mmol) were dissolved in dry methanol (10 ml) and stirred at room temperature for 8 hours (Scheme-1). A yellow colored compound precipitated out from the reaction mixture. The precipitate was filtered, washed with cold methanol (2 x 5 ml) and diethyl ether (3 x 10 ml) and dried in vacuum.

2.5.1. [(p-cymene)Ru{pyC(CN)NO}Cl] (1)

Yield: 62 mg (74%); IR (KBr, cm^{-1}): 2959(m), 2203(m), 1603(m), 1482(m), 1443(m), 1396(s), 1368(m), 871(m), 788(m); ^{1}H NMR (400 MHz, DMSO-d_6): δ = 9.20 (d, 1H, *J* = 8.0 Hz , $CH_{(py)}$), 7.94 (t, 1H, $CH_{(py)}$), 7.38 (t, 1H, $CH_{(py)}$), 7.30 (d, 1H, *J* = 8.0 Hz, $CH_{(py)}$), 1.01 (dd. 6H, *J* = 8 and 8 Hz, $CH_{(p\text{-cym})}$), 2.07 (s, 3H, $CH_{(p\text{-cym})}$), 2.62 (sept, 1H, $CH_{(p\text{-cym})}$), 5.60 (d, 1H, J = 8.0 Hz, $CH_{(p\text{-cym})}$), 5.68 (d, 1H, *J* = 4.0, $CH_{(p\text{-cym})}$), 5.80 (d, 1H, *J* = 8.0, $CH_{(p\text{-cym})}$), 5.87 (d, 1H, *J* = 8.0 Hz, $CH_{(p\text{-cym})}$); HRMS-APCI (m/z): 417.0302 $(M+H)^+$; UV-Vis { Acetonitrile, λ_{max} nm ($\varepsilon/10^{-4}$ M^{-1} cm^{-1})}: 237 (1.83), 302 (1.18), 370 (0.61); Anal. Calc for $C_{17}H_{18}ClN_3ORu$ (416.86); C, 48.98; H, 4.35; N, 10.08. Found: C, 49.14; H, 4.42; N, 10.23 %.

*2.5.2. [Cp*Rh{pyC(CN)NO}Cl] (2)*

Yield: 66 mg (78%); IR (KBr. cm^{-1}): 2918(m), 2212(m), 1602(m), 1481(m), 1444(m), 1398(s), 1372(s), 1155(m), 766(m); ^{1}H NMR (400 MHz, DMSO- d_6): δ = 8.54 (d, 1H, *J* = 4.0 Hz, $CH_{(py)}$), 7.88 (t, 1H, $CH_{(py)}$), 7.40 (t, 1H, $CH_{(py)}$), 7.31 (d, 1H, *J* = 8.0 Hz, $CH_{(py)}$), 1.59 (s, 15H, $CH_{(Cp^*)}$); HRMS-APCI (m/z): 420.0451 $(M+H)^+$; UV-Vis { Acetonitrile, λ_{max} nm ($\varepsilon/10^{-4}$ M^{-1} cm^{-1})}: 236 (1.78), 255 (1.35), 289 (1.08), 374 (0.71); Anal. Calc for $C_{17}H_{19}ClN_3ORh$ (419.71); C, 48.65; H, 4.56; N, 10.01. Found: C, 48.68; H, 4.62; N, 10.18 %.

*2.5.3. [Cp*Ir{pyC(CN)NO}Cl] (3)*

Yield: 80 mg (78%); IR (KBr. cm^{-1}): 2922(m), 2204(m), 1605(w), 1483(m), 1394(s), 1368(s), 765(m); ^{1}H NMR (400 MHz, DMSO-d_6): δ = 8.54 (d, 1H, *J* = 4.0 Hz, $CH_{(py)}$), 7.80 (t, 1H, $CH_{(py)}$), 7.52 (d, 1H, *J* = 4 Hz, $CH_{(py)}$), 7.23 (t, 1H, $CH_{(py)}$), 1.62 (s, 15H, $CH_{(Cp^*)}$); HRMS-APCI (m/z): 510.0824 $(M+H)^+$; UV-Vis { Acetonitrile, λ_{max} nm ($\varepsilon/10^{-4}$ M^{-1} cm^{-1})}: 233 (1.46), 288 (0.96), 378 (0.53); Anal. Calc for $C_{17}H_{19}ClN_3OIr$ (509.02); C, 40.11; H, 3.76; N, 8.26. Found: C, 40.28; H, 3.88; N, 8.38 %.

*2.6. General procedure for synthesis of cationic complex (**4-9**)*

A mixture of starting metal precursor (0.1 mmol) and ligand 2-pyridyl phenyloxime {pyC(Ph)NOH} or 2-thiazolyl methyloxime {tzC(Me)NOH} (0.2 mmol) and 2.5 equivalents of NH_4PF_6 were dissolved in dry methanol (10 ml) and stirred at room temperature for 8 hours (Scheme-2 and 3). The solvent was evaporated the residue was dissolved in dichloromethane and filtered through celite, the filtrate was concentrated to 1 ml and excess hexane was added to precipitate the compound. The precipitate was collected and dried in vacuum.

2.6.1. [(p-cymene)Ru{pyC(Ph)NOH}Cl](PF$_6$) (4)

Yield: 96 mg (78%); IR ((KBr. cm^{-1}): 3314(b), 3090(s), 2967(w), 1598(s), 1472(s), 1366(m), 1192(s), 1031(s) 838(s); ^{1}H NMR (400 MHz, DMSO-d_6): 9.45 (d, 1H, J = 8.0 Hz, $CH_{(py)}$), 8.04 (t, 1H, $CH_{(py)}$), 7.66 (t, 1H, $CH_{(py)}$), 7.54-7.59 (m, 3H, $CH_{(py),\ (Ar)}$), 7.29-7.32 (m, 3H, $CH_{(Ar)}$), 1.06 (d 3H, J = 8.0 Hz, $CH_{(p\text{-cym})}$), 1.13 (d, 3H, J = 8.0 Hz, $CH_{(p\text{-cym})}$), 2.26 (s, 3H, $CH_{(p\text{-cym})}$), 2.70 (sept, 1H, $CH_{(p\text{-cym})}$), 5.72 (d, 1H, J = 8.0 Hz, $CH_{(p\text{-cym})}$), 6.02 (d, 1H, J = 8.0 Hz, $CH_{(p\text{-cym})}$), 6.12 (d, 1H, J = 8.0 Hz, $CH_{(p\text{-cym})}$), 6.19 (d, 1H, J = 8.0 Hz, $CH_{(p\text{-cym})}$), OH not observed; HRMS-APCI (m/z): 469.0652 $(M\text{-}PF_6)^+$; UV-Vis {Acetonitrile, λ_{max} nm ($\varepsilon/10^{-4}$ M^{-1} cm^{-1})}: 233 (2.28), 272 (0.95), 376 (0.29); Anal. Calc for $C_{22}H_{24}ClF_6N_2OPRu$ (613.93); C, 43.04; H, 3.94; N, 4.56. Found: C, 43.21; H, 4.06; N, 4.63 %.

2.6.2. [Cp*Rh{pyC(Ph)NOH}Cl](PF$_6$) (5)

Yield: 108 mg (87%); IR (KBr. cm^{-1}): 3314(b), 3112(m), 2922(m), 1595(s), 1470(w), 1378(w), 1189(s), 1027(s), 841(s); ^{1}H NMR (400 MHz, DMSO-d_6): δ = 8.77 (d, 1H, J = 4.0 Hz, $CH_{(py)}$), 8.06 (t, 1H, $CH_{(py)}$), 7.77 (t, 1H, $CH_{(py)}$), 7.59-7.63 (m, 3H, $CH_{(py),\ (Ar)}$), 7.40-7.45 (m, 3H, $CH_{(Ar)}$), 1.77 (s, 15 H, $CH_{(Cp^*)}$), OH not observed; HRMS-APCI (m/z): 471.0721 $(M\text{-}PF_6)^+$; UV-Vis {Acetonitrile, λ_{max} nm ($\varepsilon/10^{-4}$ M^{-1} cm^{-1})}: 266 (0.75), 357 (0.30); Anal. Calc for $C_{22}H_{25}ClF_6N_2OPRh$ (616.77); C, 42.84; H, 4.09; N, 4.54. Found: C, 42.91; H, 3.96; N, 4.67 %.

*2.6.3. [Cp*Ir{pyC(Ph)NOH}Cl](PF$_6$) (6)*

Yield: 110 mg (78%); IR (KBr. cm^{-1}): 3438(b), 3137(m), 2975(m), 1624(s), 1457(w), 1378(w), 1142(s), 1033(s), 843(s); ^{1}H NMR (400 MHz, DMSO-d$_6$): δ = 8.78 (d, 1H, *J* = 4.0 Hz, CH$_{(py)}$), 7.92 (t, 1H, CH$_{(py)}$), 7.79 (t, 1H, CH$_{(py)}$), 7.48-7.53 (m, 3H, CH$_{(py),\ (Ar)}$), 7.43-7.47 (m, 3H, CH$_{(Ar)}$), 1.77 (s, 15 H, CH$_{(Cp*)}$), OH not observed; HRMS-APCI (m/z): 561.1283 (M-PF$_6$)$^+$; UV-Vis {Acetonitrile, λ_{max} nm (ε/10^{-4} M^{-1} cm^{-1})}: 296 (0.78), 360 (0.59); Anal. Calc for $C_{22}H_{25}ClF_6N_2OPIr$ (706.08); C, 37.42; H, 3.57; N, 3.97. Found: C, 37.58; H, 3.65; N, 4.11 %.

2.6.4. [(p-cymene)Ru{tz(CH$_3$)NOH}Cl](PF$_6$) (7)

Yield: 88 mg (79%); IR (KBr. cm^{-1}): 3594(s), 3429(b), 3109(m), 2970(m), 1631(s), 1505(m), 1471(w), 1381(s), 1140(s), 1040(m), 846(s); ^{1}H NMR (400 MHz, DMSO-d$_6$): δ = 11.3 (s, 1H, OH), 8.50 (d, 1H, *J* = 4.0 Hz, CH$_{(tz)}$) 7.89 (d, 1H, *J* = 8.0 Hz, CH$_{(tz)}$), 2.52 (s, 3H, CH$_3$), 1.10 (d, 3H, *J* = 8 Hz, CH$_{(p\text{-cym})}$), 1.18 (d, 1H, *J* = 8 Hz, CH$_{(p\text{-cym})}$), 2.29 (s, 3H, CH$_{(p\text{-cym})}$), 2.75 (sept, 1H), 6.06 (d, 1H, *J* = 4 Hz, CH$_{(p\text{-cym})}$), 5.89 (d, 2H, *J* = 8 Hz, CH$_{(p\text{-cym})}$), 5.64 (d, 1H, *J* = 4 Hz, CH$_{(p\text{-cym})}$); HRMS-APCI (m/z): 413.0118 (M-PF$_6$)$^+$; UV-Vis {Acetonitrile, λ_{max} nm (ε/10^{-4} M^{-1} cm^{-1})}: 297 (0.48), 350 (0.32); Anal. Calc for $C_{15}H_{20}ClF_6N_2OPRuS$ (557.88); C, 32.29; H, 3.61; N, 5.02. Found: C, 32.41; H, 3.69; N, 5.13 %.

*2.6.5. [Cp*Rh{tzC(CH$_3$)NOH}Cl](PF$_6$) (8)*

Yield: 84 mg (75%); IR (KBr. cm^{-1}): 3618(s), 3433(b), 3138(m), 2824(w), 1598(s), 1470(w), 1382(w), 1139(m), 1027(w), 842(s); ^{1}H NMR (400 MHz, DMSO-d$_6$): δ = 11.81 (s, 1H, OH), 8.14 (d, 1H, *J* = 4 Hz, CH$_{(tz)}$), 8.08 (d, 1H, *J* = 4 Hz, CH$_{(tz)}$), 2.56 (s, 3H, CH$_3$), 1.78 (s, 15 H, CH$_{(Cp*)}$); HRMS-APCI (m/z): 415.0131 (M-PF$_6$)$^+$; UV-Vis { Acetonitrile, λ_{max} nm (ε/10^{-4} M^{-1} cm^{-1})}: 230 (0.53), 287 (0.35), 351 (0.32); Anal. Calc for $C_{15}H_{21}ClF_6N_2OPRhS$ (560.73); C, 32.13; H, 3.77; N, 5.00. Found: C, 32.19; H, 3.85; N, 5.12 %.

222 ***2.6.6. [Cp*Ir{tzC(CH$_3$)NOH}Cl](PF$_6$) (9)***

223 Yield: 100 mg (77%); IR (KBr. cm^{-1}): 3619(s), 3339(b), 3136(m), 2926(m), 1599(m), 1458(m),
224 1387(m), 1144(w), 1036(m), 844(s); ^{1}H NMR (400 MHz, DMSO-d$_6$): δ = 11.81 (s, 1H, OH),
225 8.25 (d, 1H, *J* = 4 Hz, CH$_{(tz)}$), 8.23 (d, 1H, *J* = 4 Hz, CH$_{(tz)}$), 2.58 (s, 3H, CH$_3$), 1.77 (s, 15 H,
226 CH$_{(Cp^*)}$); HRMS-APCI (m/z): 505.0761 (M-PF$_6$)$^+$; UV-Vis {Acetonitrile, λ_{max} nm (ε/10^{-4} M^{-1} cm^{-1})}: 290 (0.76), 360 (0.346); Anal. Calc for C$_{15}$H$_{21}$ClF$_6$N$_2$OPIrS (650.04); C, 27.72; H, 3.26; N,
228 4.31. Found: C, 27.90; H, 3.32; N, 4.41 %.

229 **3. Results and discussion**

230 *3.1. Synthesis of the complexes*

231 The neutral metal oximato complexes (**1**-**3**) were isolated by the reaction of metal
232 precursors with 2-pyridyl cyanoxime. The neutral metal complexes were formed as a result of
233 deprotonation of the oxime hydrogen as confirmed by spectroscopic and X-ray diffraction
234 studies. It is assumed that the presence of the cyano group as a substituent in 2-pyridyl
235 cyanoxime increases its acidity leading to its deprotonation and resulting in elimination of HCl.
236 Furthermore deprotonation of oxime hydrogen generates an anionic charge on oxime-O which
237 was found to be delocalized over the 2-pyridyl cyanoxime moiety as reflected from the bond
238 lengths values (Table 2). The cationic metal oxime complexes (**4**-**9**) were prepared by the
239 reaction of metal precursors with 2-pyridyl phenyloxime and 2-thiazolyl methyloxime.
240 Deprotonation of oxime hydrogen was not observed in this case with phenyl and methyl as
241 substituent. The cationic complexes were isolated with PF$_6$ counter ion. All these complexes
242 were isolated as yellow solids except complexes (**6** and **9**) which were isolated as orange solids.
243 These complexes are non-hygroscopic, stable in air as well as in solid state. They are soluble in
244 common organic solvents like acetone, acetonitrile, dichloromethane and DMSO but insoluble in

hexane and diethyl ether. All these complexes were fully characterized by spectroscopic techniques.

3.2. Spectral studies of the complexes

The IR spectra of all the complexes shows characteristic stretching frequencies for C=N and C=C around 1450-1620 cm^{-1} and these values are shifted to higher frequencies as compared to the free ligand following coordination of the ligand to the metal atom. The C≡N stretching frequencies for the neutral complexes (**1**-**3**) appeared in the lower frequency region around 2204-2212 cm^{-1} as compared to the free ligand at 2229 cm^{-1} which may be due to delocalization of the anionic charge on oxime-O. The disappearance of the OH stretching frequency around 3100-3400 cm^{-1} in the neutral complexes (**1**-**3**) indicates the deprotonation of the oxime hydrogen, which is also confirmed from the crystal structures. The presence of the OH stretching frequency around 3100-3450 cm^{-1} in cationic complexes (**4**-**9**) suggests that the binding occurs through the nitrogen atom. In addition, the cationic metal complexes (**4**-**9**) displayed a strong intense band around 838-849 cm^{-1} corresponding to the P-F stretching frequency of the counter ion [49].

In the ^{1}H NMR spectra of the complexes the signals for the aromatic protons of the ligand was observed in the downfield region around 7.32-9.50 ppm. The shift of the ligand resonance signals clearly indicates the coordination of the ligand to the metal ion. The disappearance of the OH proton signal in the neutral complexes (**1**-**3**) as compared to the free ligand at 13.02 ppm indicates the deprotonation of the hydroxyl proton. The OH proton resonance for complexes (**7**-**9**) was observed as singlet around 11.3-11.9 ppm respectively. Besides these resonance signals for the aromatic part of the ligand complexes (**1**, **4** and **7**) displayed an unusual pattern of signal for the *p*-cymene moiety. The aromatic proton signal for the *p*-cymene ligand showed four doublets for complexes (**1**) and (**4**) at around 5.60-6.19 ppm and three doublets for complex (**7**)

around 5.64-6.06 ppm instead of two doublets in the starting metal precursor. And also methyl protons of isopropyl group displayed two doublets for complex (**4**) and (**7**) and one doublet of doublet for complex (**1**) around 1.01-1.18 ppm instead of one doublet in the metal precursor. This surprising pattern of signals is due to desymmetrization of the *p*-cymene ligand upon coordination of the oxime ligand and these results are in good agreement with similar reported complexes [50]. Complexes (**1**, **4** and **7**) displayed septet and singlet around 2.07-2.75 ppm corresponding to the methine protons of the isopropyl group and methyl group of the *p*-cymene ligand. The methyl proton resonance for complexes (**8**) and (**9**) was observed as a singlet at 2.56 and 2.58 ppm. In addition, to all these signals a strong peak for the Cp*Rh complexes (**2**, **5** and **8)** and the Cp*Ir complexes (**3**, **6** and **9)** was observed between 1.59-1.78 ppm for the methyl protons of the pentamethylcyclopentadienyl ligand.

In the mass spectra of the neutral complexes (**1-3**), the molecular ion peak was observed as $(M+H)^+$ ion peak at m/z: 417.0302, m/z: 420.0451 and m/z: 510.0824 respectively. Whereas the mass spectra of the cationic complexes (**4-9**) displayed their molecular ion peaks at m/z: 469.0652, m/z: 471.0721, m/z: 561.1283, m/z: 413.0118, m/z: 415.0131 and m/z: 505.0761 which corresponds to the $[M-PF_6]^+$ ion. The mass spectra values of the complexes strongly support the formation of the complexes.

The absorption spectra of the complexes were recorded in acetonitrile at 10^{-4} M concentration at room temperature and the plot is shown in (Figure S1). The electronic spectra of the complexes display absorption band in the higher energy region around 230-305 nm which can be assigned as ligand centered π-π* and n-π*transition [51]. The low spin Ru(II), Rh(III) and Ir(III) complexes provides filled dπ (t_{2g}) orbitals of proper symmetry which can interact with low lying π* orbitals of the ligand. Therefore a metal to ligand charge transfer (MLCT) band is

expected in their absorption spectra. The bands in the lower energy region around 350-380 nm can be assigned as metal to ligand charge transfer (MLCT) dπ(M) to π^*(L) transition [52].

3.3. Molecular structures of complexes

The molecular structures of some of the respective complexes were established by single crystal X-ray analysis. Suitable single crystals were attached to a glass fiber and transferred into the Oxford Diffraction Xcalibur Eos Gemini diffractometer. The crystallographic details and structure refinement details are summarized in Table 1. The geometrical parameters around the metal atom involving ring centroid are listed in Table 2. Complex (**1**) crystallized in orthorhombic system with space group *Pca2₁*. Complexes (**2**, **3** and **8)** crystallized in monoclinic crystal system with space group *P2₁/c* whereas complexes (**4**) and (**7**) crystallized with *P2₁/n* and *P2₁/m* space group in monoclinic crystal system. Complex (**5**) crystallized in triclinic system with space group *P* $\bar{1}$.

The molecular structures of the complexes revealed a typical three legged "piano stool" geometry about the metal center with the metal atom coordinated by the arene/Cp* ring in a η^6/ η^5 manner, two nitrogen donor atoms from chelating ligand in a bidentate κ^2 NN′ fashion and one chloride atom. The metal atom in these complexes is situated in a pseudo-octahedral arrangement with the ligand coordinating through the pyridine and oxime nitrogen atom forming a five membered metallocyclic ring. The bite angle values N(1)-Ru(1)-N(2) in ruthenium complexes are 77.81(13) (**1**), 75.66(7) (**4**) and 78.0(10) (**7**). The average Ru-C distances in complexes (**1**) and (**4**) are almost equal 2.203 and 2.205 Å, while in complex (**7**) the Ru-C distance is 2.179 Å. The Ru-centroid of the arene ring distances in complexes (**1**) and (**4**) are equal 1.696 Å while in complex (**7**) it is slightly longer 1.728 Å. The bite angle values N(1)-M(1)-N(2) in rhodium and iridium complexes are 78.06(16) (**2**), 78.0(3) (**3**), 74.92(11) (**5**) and 75.16(15) (**8**). The average

M-C distances (where M = Rh/Ir) are {2.165 (**2**), 2.170 (**3**), 2.157 (**5**) and 2.149 (**8**) Å} while the distance between the metal to centroid of the Cp* ring is found to be in the range of 1.775-1.803 Å respectively. The M-N and M-Cl bond distances (where M = Ru, Rh and Ir) in all these complexes are found to be in close agreement with previously reported values for ruthenium, rhodium and iridium complexes with NN′ donor ligands [53]. Surprisingly, the molecular structures of complexes (**1**, **2** and **3**) revealed the deprotonation of the oxime hydrogen generating an anionic charge on oxime-O. This anomalous behavior of deprotonation of the oxime hydrogen is not surprising as the presence of electron withdrawing cyano group increases the acidity of the oxime fragment. It was further observed that the anionic charge on the oxime-O was delocalized over the 2-pyridyl cyanoxime moiety. This is supported by the oximate C(6)-N(2) {1.330(5) (**1**), 1.334(7) (**2**) and 1.360(11) (**3**) Å} and N(2)-O(1) {1.271(4) (**1**), 1.262(5) (**2**) and 1.254(9) (**3**) Å} bond lengths which is slightly larger and smaller than the corresponding C-N {1.287(2) Å} and N-O {1.367(2) Å} bond in the free ligand indicating their partial double bond character and delocalization of the anionic charge (Scheme-1) [54]. These results are further supported by the theoretical calculations as well (Table S1). A similar pattern of delocalization of charge was reported for the cyclometalated iridium complex $[Ir(ppy)_2(pyald)]$ (ppy = 2-phenylpyridine, pyald = 2-pyridinealdoxime) where the anionic charge was delocalized over the pyridine aldoxime moiety [55]. The positive charge of the ruthenium atom in complex (**1**) is balanced by one negative charge from chloride ion and one negative charge from the oxime-O. Similarly in complexes (**2**) and (**3**), the positive charge of the metal atom is balanced by one anionic charge from Cp* ligand, one chloride ion and anionic oxime-O.

Further the crystal structure of complex (**1**) displayed three different types of intermolecular hydrogen bonding; the first between the anionic oxime-O and hydrogen atom

from pyridine (2.393 Å), the second between the oxime-O and methine hydrogen (2.383 Å) and third from the aromatic hydrogen of *p*-cymene ligand (2.531 Å). Also C-H····Cl (2.848 Å) interaction between the chloride atom and H-atom of pyridine ring (Figure S2) has been observed. Crystal structure of complex (**2**) exhibits two different types of C-H·····Cl (2.813 and 2.902 Å) interactions between the chloride atom attached to metal and H-atom of Cp* group and pyridine and also C-H·····π (2.904 Å) interaction was observed between the methyl-H atom and Cp* group (Figure S3). The crystal structure of complex (**3**) is stabilized by C-H·····π (2.756 Å) interaction between the methyl-H atom and Cp* group and C-H·····Cl (2.917 Å) interaction between chloride atom and methyl H atom of Cp*. It also exhibits two types of intermolecular hydrogen bonding C-H·····O (2.713 Å) between the anionic oxime-O and methyl-H of Cp* and C-H·····N (2.689 Å) interaction between nitrogen atom of cyano group and pyridine-H atom (Figure S4). The crystal packing of complex (**4**) and (**5**) forms a dimeric unit via weak intermolecular C-H·····O (2.700 and 2.848 Å) and O-H·····Cl (2.228 and 2.245 Å) interactions between the methyl-H atom of Cp* and oxime-O and oxime-H atom and chloride atom attached to metal ion (Figure S5). Further the crystal structure of complex (**8**) crystallized with one water molecule which forms four different types of intermolecular hydrogen bonding the first between the hydrogen atom of water molecule and chloride atom O-H·····Cl (2.807 Å), the second between the fluorine atom of counter ion PF_6 and H-atom of water molecule O-H·····F (2.319 Å), the third between the O-atom and H-atom of Cp* group C-H·····O (2.507 Å) and the last between the O-atom and H-atom of oxime moiety O-H·····O (1.829 Å) (Figure S6). These weak interactions play an important role in the formation of supramolecular motifs.

3.4. Chemosensitivity studies

The oximato and oxime metal complexes (**1**-**9**) were tested for their *in vitro* activity against two cancer cell lines HT-29 (human colorectal cancer) and MIAPaCa-2 (human pancreatic cancer) using the MTT assay. The response of the cell line HT-29 and MIAPaCa-2 to the test complexes (**1**-**9**) and cisplatin is presented in graphical form in Figure 4 and in tabular form in Table 3. Complexes (**1**) and (**8**) were found to be inactive against both the cell line with IC_{50} values > 100 μM. Complexes (**4**) and (**5**) were found to be less active against HT-29 cell line whereas complex (**4**) was found to be more active against MIAPaCa-2 cell line. In contrast complexes (**2**) and (**7**) displayed moderate activity against both cell lines with IC_{50} value in the range of 8.28 to 23.74 μM. However, among all the ruthenium, rhodium and iridium complexes, the iridium complexes (**3**), (**6**) and (**9**) with cyano, phenyl and methyl substituted oximes displayed high cytotoxicity. The iridium complexes were found to be highly active against HT-29 cancer cell line with IC_{50} values in the range of 5.82 to 10.54 μM. Also, the iridium complexes exhibits high potency against MIAPaCa-2 cell line with IC_{50} values ranging from 2.89 to 9.65 μM. However among all the iridium complexes, the iridium oximato compound (**3**) with cyano substituent was found to be the most potent towards MIAPaCa-2 cell line (IC_{50} = 2.87 ± 0.26 μM) with IC_{50} value comparable to that of cisplatin (IC_{50} = 2.84 ± 2.05 μM). This high remarkable activity of the iridium based complexes suggests that the presence of the substituent in the chelating ligand plays a crucial role and affects the cytotoxicity [8]. This study demonstrates that the cytotoxicity of the complexes can be finely tuned by changing the nature and position of the substituent in the chelating ligand without changing the arene systems.

3.5. Optimized structural geometry

The comparison of the geometric parameters (selected bond lengths and bond angles) of the optimized structures and the crystal structures of the complexes (**1**-**9**) are listed in Table S1.

The calculated bond lengths and the bond angles of the complexes are in good agreement with the experimental data indicating the reliability of the theoretical method (B3LYP/6-31G**/LanL2DZ) used in the present study. It should be noted that a slight discrepancy from the experimental value in N(2)-Ru(1)-Cl(1), N(1)-Ru(1)-Cl(1) and N(2)-Rh(1)-Cl(1) bond angle for complexes (**1**), (**4**) and (**8**) has been observed (Table S1).

3.6. Molecular electrostatic potential (MESP)

MESP is an important quantity to understand sites for electrophilic attack and nucleophilic attack as well as hydrogen bond interactions [56, 57]. The MESP diagram for all the complexes are shown in Figure 5. The red region represents the negative electrostatic potential, which is related to the nucleophilic reactivity whereas the blue regions represents the positive electrostatic potential and is related to the electrophilic reactivity. The red regions in complexes containing 2-pyridyl cyanoxime and 2-pyridyl phenyloxime does not change much drastically, but in complexes containing 2-thiazolyl methyloxime, the intensity of red color decreases slightly in complexes (**8)** and (**9**) as compared to complex (**7**).

3.7. Charge Distribution

The charges on the selected atoms as obtained from NBO analysis are listed in Table S2. The charge on the metal (Ru, Rh and Ir) for complexes (**1**-**9**) ranges between -0.028 e (complex **7**) and 0.0248 e (complex **3**), which are less than their formal charges of +2 (Ru) and +3 (Rh/Ir). Moreover, as indicated in Table S2, the negative charge on the N1 decreases in all the complexes as compared to their charge in isolated ligands. These results confirm that the ligands transfer their negative charges to the metal on complex formation. The charge on the chloride atom for all the complexes ranges between -0.342 e and -0.406 e. It should be noted that the negative charges on chloride for ruthenium complexes are comparatively lower whereas it is higher for rhodium and iridium complexes. These lowering of charges in ruthenium complexes are the

reflection of the negative charges on ruthenium complex (**1**) and (**7**) and very small positive charge of 0.002 e on Ru in complex (**4**). As observed from the experimental results, that in the neutral complexes (**1**, **2** and **3**) the anionic charge on oxime-O was delocalized over the 2-pyridyl cyanoxime moiety, therefore we further tried to justify these results with theoretical data as well. In isolated ligand, 2-pyridyl cyanoxime, the charges on the O1, N2 and C6 are found to be -0.545, -0.037 and 0.062 e. On complex formation, the negative charges on the O1 and N2 decreases and attains a value of -0.381, -0.387, -0.403 e and 0.159, 0.126, 0.107 e respectively, whereas C6 attains negative charges of -0.050, -0.036 and -0.036 e (Table S2). These results confirm that the anionic charge on the oxime-O is delocalized on complex formation. Moreover, as seen from the bond lengths values (Table 2), on complex formation, the N2-O1 bond is shortened and attains a partial double bond character whereas the N2-C6 bond is elongated as compared to the bonds in isolated ligand.

3.8. Frontier Molecular Orbital and Absorption spectra

It is well known that the frontier molecular orbitals (HOMO and LUMO) help in characterizing the electron donating and electron accepting ability of a molecule. Moreover, the HOMO-LUMO energy gap has been utilized as an important parameter to understand the reactivity of a molecule. A lower HOMO-LUMO gap means lesser stability and higher reactivity whereas for higher HOMO-LUMO gap, it is the reverse case. The details of the frontier molecular orbitals are shown in Figure 6 where the red and the green regions represent the positive and the negative phase respectively. The energy gap is least for complex (**6**) whereas it is highest for complex (**8**). It should be noted that the energy gap is less for the complexes containing 2-pyridyl phenyloxime indicating its less stability and greater reactivity as compared to the complexes containing ligand 2-pyridyl cyanoxime and 2-thiazolyl methyloxime. The % composition of molecular orbital analysis as shown in Table S3, predicts that for the complexes

containing 2-pyridyl cyanoxime (complexes **1**, **2** and **3**), the maximum percentage of HOMO i.e. 42%, 35% and 39% is located on the ligand itself. The same case can be encountered for complexes (**7**) and (**8**) as well whereas for complexes (**4**), (**6**) and (**9**) most percentage of HOMO is located on the metal (Table S3). On the other hand, the LUMO is located mainly on the ligand for almost all the complexes except for complex (**2**), where it is located on the Rh metal (about 37%).

The electronic absorption spectra were calculated using the TD-DFT method in acetonitrile solvent employing PCM model. The calculated and the experimental absorption data, HOMO-LUMO energy gaps, and the character of electronic transitions are listed in Table 4. The H→L transitions for complexes (**1**), (**3**), (**7**) and (**8**) occurring at 492, 468, 450 and 485 nm corresponds to ILCT character, for complexes (**4**), (**6**) and (**9**) at 453, 464 and 463 nm corresponds to MLCT character whereas for complexes (**2**) and (**5**) at 512.44 and 477 nm corresponds to LMCT and LLCT character. These MLCT character can be assigned as dπ(M)→π*(L) transitions, ILCT character are for π→π* transitions and LLCT for Pπ(Cl)→π*(L) transitions. In agreement with the experimental results, few MLCT transitions has also been observed at 357 nm (**4**), 359, 335 nm (**7**), 336 nm (**8**) and 350 nm (**9**). Further, few ILCT and LLCT transitions have been observed between 230-304 nm which are in well agreement with the experimental data.

4. **Conclusion**

In summary, we have successfully synthesized ruthenium, rhodium and iridium half-sandwich oximato and oxime complexes. These complexes were full characterized by various spectroscopic studies and X-ray analysis. The ligands under study preferably bind to the metal in a bidentate κ^2 NN′ fashion using pyridine and oxime nitrogen atom. X-ray structure of

complexes (**1-3**) reveals the deprotonation of the oxime hydrogen atom leading to the formation of neutral complexes. Chemosensitivity activity of the complexes carried out against HT-29 and MIAPaCa-2 cancer cell lines displayed that some of the complexes are cytotoxic however iridium-based complexes displayed more potency than ruthenium and rhodium complexes. In particularly the neutral iridium oximato compounds possessed the highest activity among other cationic iridium oxime complexes. Further, TD-DFT calculated absorption spectral data are in well agreement with experimental results.

Acknowledgements

Sanjay Adhikari and Dipankar Sutradhar thanks UGC, New Delhi, India for providing financial assistance in the form of university fellowship (UGC-Non-Net). We thank DST-PURSE SCXRD, NEHU-SAIF, Shillong, India for providing Single crystal X-ray analysis and other spectral studies. AKC thanks Computer center, NEHU, for computational facilities.

Appendix A. Supplementary data

CCDC **1486252** (**1**), **1486253** (**2**), **1486254** (**3**), **1486255** (**4**), **1486256** (**5**), **1486257** (**7**) and **1486258** (**8**) contains the supplementary crystallographic data for this paper. These data can be obtained free of charge via www.ccdc.cam.ac.uk/data_request/cif, by e-mailing data_request@ccdc.cam.ac.uk, or by contacting The Cambridge Crystallographic Data Centre, 12, Union Road, Cambridge CB2 1EZ, UK; Fax: +44 1223 336033.

References

[1] A.A. Nazarov, C.G. Hartinger, P.J. Dyson, J. Organomet. Chem. 751 (2014) 251.

[2] B. Therrien, Coord. Chem. Rev. 253 (2009) 493.

[3] L. Ronconi, P.J. Sadler, Coord. Chem. Rev. 251 (2007) 1633.

[4] A.F.A. Peacock, P.J. Sadler, Chem. Asian J. 3 (2008) 1890.

[5] A.L. Noffke, A. Habtemariam, A.M. Pizarro, P.J. Sadler, Chem. Comm. 48 (2012) 5219.

[6] Y. Geldmacher, M. Oleszak, W.S. Sheldrick, Inorg. Chim. Acta 393 (2012) 84.

[7] G.Suss-Fink, Dalton Trans. 39 (2010) 1673.

[8] A.J. Millett, A. Habtemariam, I. Romero-canelon, G.J. Clarkson, P.J. Sadler, Organometallics, 34 (2015) 2683.

[9] Z. Almodares, S.J. Lucas, B.D. Crossley, A.M. Basri, C.M. Pask, A.J. Hebden, R.M. Philips, P.C. McGowan, Inorg. Chem. 53 (2014) 727.

[10] Y.K. Yan, M. Melchart, A. Habtemariam, P.J. Sadler, Chem. Commun. (2005) 4764.

[11] C.G. Hartinger, N. Metzler-Nolte, P.J. Dyson, Organometallics, 31 (2012) 5677.

[12] R.E. Morris, R.E. Aird, P.S. Murdoch, H. Chen, J. Cummings, N.D. Hughes, S. Parsons, A. Parkin, G. Boyd, D.I. Jodrell, P.J. Sadler, J. Med. Chem. 44 (2001) 3616.

[13] M. Martinez-Alonso, N. Busto, F.A. Jalon, B.R. Manzano, J.M. Leal, A.M. Rodriguez, B. Garcia, G. Espino, Inorg. Chem. 53 (2014) 11274.

[14] Z. Liu, A. Habtemariam, A.M. Pizarro, S.A. Fletcher, A. Kisova, O. Vrana, L. Salassa, P.C.A. Bruijnincx, G.J. Clarkson, V. Brabec, P.J. Sadler, J. Med. Chem. 54 (2011) 3011.

[15] A. Habtemariam, M. Melchart, R. Fernandez, S. Parsons, I.D.H. Oswald, A. Parkin, F.P.A. Fabbiani, J.E. Davidson, A. Dawson, R.E. Aird, D.I. Jodrell, P.J. Sadler, J. Med. Chem. 49 (2006) 6858.

[16] S.J. Lucas, R.M. Lord, A.M. Basri, S.J. Allison, R.M. Phillips, A.J Blacker, P.C. McGowana, Dalton Trans. 45 (2016) 6812.

[17] B. Lastra-Barreira, J. Diez, P. Crochet, I. Fernandez, Dalton Trans. 42 (2013) 5412.

[18] J.M. Hearn, I. Romero-Canelon, B. Qamar, Z. Liu, I. Hands-Portman, P.J. Sadler, Chem. Biol. 8 (2013) 1335.

[19] H. Turkmen, I. Kani, B. Cetinkaya, Eur. J. Inorg. Chem. (2012) 4494.

[20] J. DePasquale, I. Nieto, L.E. Reuther, C.J. Herbst-Gervasoni, J.J. Paul, V. Mochalin. M. Zeller, C.M. Thomas, A.W. Addison, E.T. Papish, Inorg. Chem. 52 (2013) 9175.

[21] N. Hofmann, L. Ackermann, J. Am. Chem. Soc. 135 (2013) 5877.

[22] (a) G. Gupta, S. Gloria, S.L. Nongbri, B. Therrien, K.M. Rao, J. Organomet. Chem. 696 (2011) 2014; (b) M. Kalidasan, S.H. Forbes, Y. Mozharivskyj, K.M. Rao, Inorg. Chim. Acta 421 (2014) 218; (c) S. Sangilipandi, D. Sutradhar, K. Bhattacharjee, W. Kaminsky, S.R. Joshi, A.K. Chandra, K.M. Rao, Inorg. Chim. Acta 441 (2016) 95.

[23] A. Chakravorty, Coord. Chem. Rev. 13 (1974) 1.

[24] C.W. Glynn, M.M. Turnbull, Trans. Met. Chem. 27 (2002) 822.

[25] N. Gerasimchuk, T. Maher, Inorg. Chem. 46 (2007) 7268.

[26] N. Gerasimchuk, A. Gamian, G. Glover, B. Szponar, Inorg. Chem. 49 (2010) 9863.

[27] C.J. Milios, T.C. Stamatatos, S.P. Perlepes, Polyhedron, 25 (2006) 134.

[28] A. Escuer, G. Vlahopoulou, S.P. Perlepes, F.A. Mautner, Inorg. Chem. 50 (2011) 2468.

[29] J. Esteban, M. Font-Bardia, J.S. Costa, S.J. Teat, A. Escuer, Inorg. Chem. 53 (2014) 3194.

[30] M. Watanabe, Y. Kashiwame, S. Kuwata, T. Ikariya, Eur. J. Inorg. Chem. (2012) 504.

[31] M. Watanabe, Y. Kashiwame, S. Kuwata, T. Ikariya, Chem. Lett. 39 (2010) 758.

[32] D.D. Perrin, W.L.F. Armarego, Purification of Laboratory Chemicals, fourth ed., Butterworths Heinemann, London, 1996.

[33] M.A. Bennett, T.N. Huang, T.W. Matheson, A.K. Smith, S. Ittel, W. Nickerson,

Inorg. Synth. 21 (1982) 74.

[34] C. White, A. Yates, P.M. Maitlis, D.M. Heinekey, Inorg. Synth. 29 (2007) 228.

[35] H. S. Jena, V. Manivannan, Inorg. Chim. Acta 394 (2013) 210.

[36] R.A. Hughes, S.P. Thompson, L. Alcaraz, C.J. Moody, J. Am. Chem. Soc. 127 (2005) 15644.

[37] G.M. Sheldrick, Acta Crystallogr. Sect. A 46 (1990) 467.

[38] G.M. Sheldrick, Acta Crystallogr. Sect. A 64 (2008) 112.

[39] L.J. Farrugia, J. Appl. Crystallogr. 32 (1999) 837.

[40] (a) A.L. Spek, PLATON, A Multipurpose Crystallographic Tool, Utrecht University, Utrecht, The Netherlands, 2008; (b) A.L. Spek, J. Appl. Crystallogr. 36 (2003) 7.

[41] R.M. Phillips, P.B. Hulbert, M.C. Bibby, N.R. Sleigh, J.A. Double, Br. J. Cancer. 65 (1992) 359.

[42] A.D. Becke, J. Chem. Phys., 98, 7 (1993) 5648.

[43] C. Lee, W. Yang, R.G. Parr, Phys. Rev., B 37, 2 (1988) 785.

[44] E. Cances, B. Mennucci, J. Tomasi, J. Chem. Phys. 107 (1997) 3032.

[45] A. E. Reed, L. A. Curtiss, F. Weinhold, Chem. Rev. 88 (1988) 899.

[46] M.E. Casida, in: J. M. Seminario (Ed.), Recent Developments and Applications in Modern Density Functional Theory, Theoretical and Computational Chemistry, vol. 4, Elsevier, Amsterdam, 1996.

[47] L. Skripnikov, Chemissian v4.36, A computer program to analyse and visualise quantum-chemical calculations, 2015.

[48] M.J. Frisch et al., GAUSSIAN 09, Revision C.01, Gaussian, Inc., Walling-ford, CT 2009.

[49] K. Nakamoto, Infrared and Raman Spectroscopy of Inorganic and Coordination Compounds, fourth ed., Wiley, New York, 1986.

[50] J.M. Gichumbi, H.B. Friedrich, B. Omondi, J. Organomet. Chem. 808 (2016) 87.

[51] N. Mohan, S. Muthumari, R. Ramesh, J. Organomet. Chem. 807 (2016) 45.

[52] G. Gupta, S. Park, S. S. Lee, J. Kim, Z. Anorg. Allg. Chem. 637, 2011, 1516.

[53] (a) K.T. Prasad, B. Therrien, K.M. Rao, J. Organomet. Chem. 693 (2008) 3049; (b) G. Gupta, S. Gloria, B. Das, K.M. Rao, J. Mol. Struc. 979 (2010) 205; (c) J.M. Gichumbi, H.B. Friedrich, B. Omondi, J. Mol. Catal. A: Chemical 416 (2016) 29; (d) L.C. Matsinha, S.F. Mapolie, G.S. Smith, Polyhedron 53 (2013) 56.

[54] A.A. Mokhir, K.V. Domasevich, N.K. Dalley, X. Kou, N.N. Gerasimchuk, O.A. Gerasimchuk, Inorg. Chim. Acta. 284 (1999) 85.

[55] S. Pal, B.C. Singh, Acta Crystallogr. E69 (2013) m159.

[56] L. Xiao-Hong, C. Hong-Ling, Z. Rui-Zhou, Z. Xian-Zhou, Spectrochim. Acta A: Mol. Biomol. Spectrosc. 137 (2015) 321.

[57] Y. Wang, Q. Liu, T. Wang, H. Yuan, J. Lin and S. Luo, 150 (2015), 902.

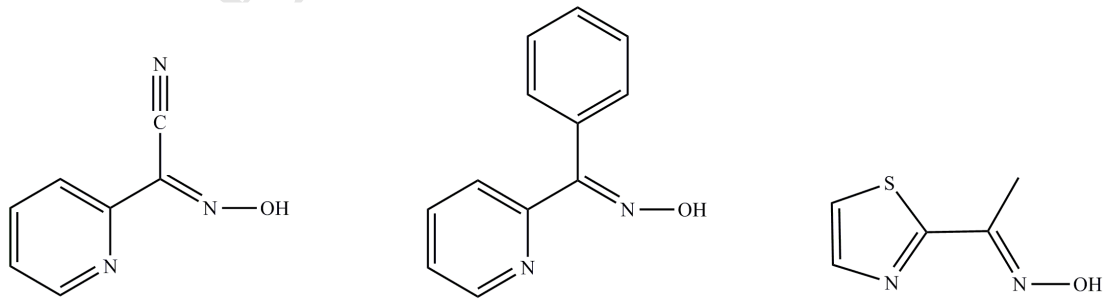

pyC(CN)NOH pyC(Ph)NOH tzC(Me)NOH

Chart-1

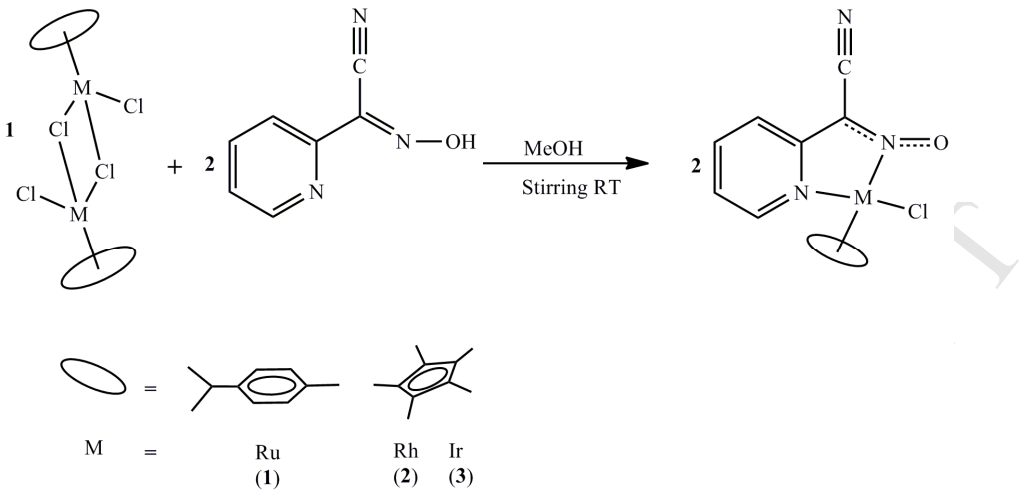

Scheme-1 Preparation of neutral complexes (**1**-**3**)

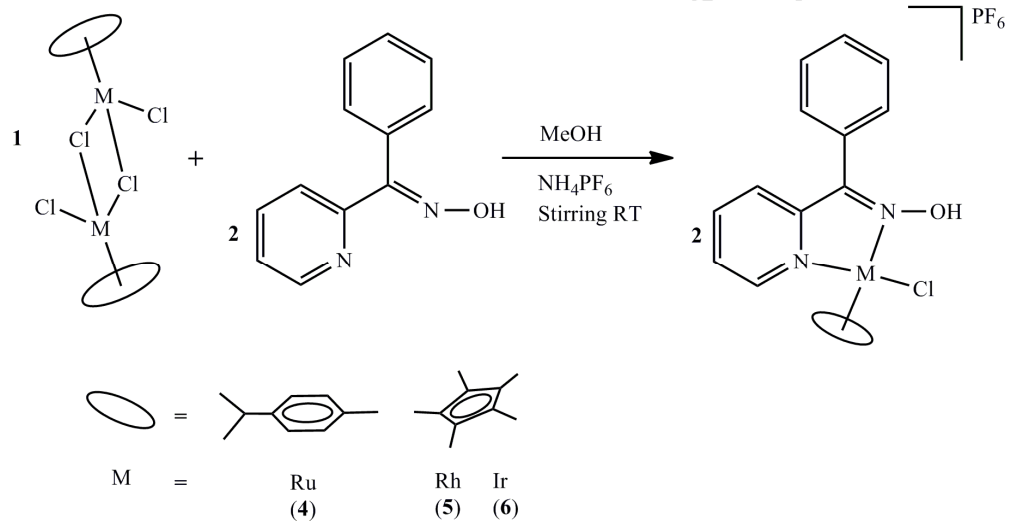

Scheme-2 Preparation of cationic complexes (**4**-**6**)

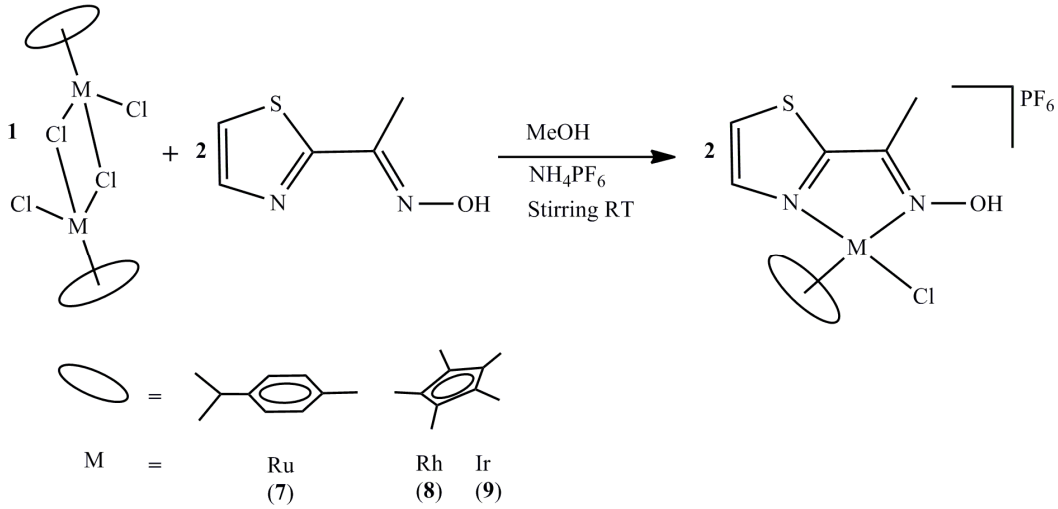

Scheme-3 Preparation of cationic complexes (**7**-**9**)

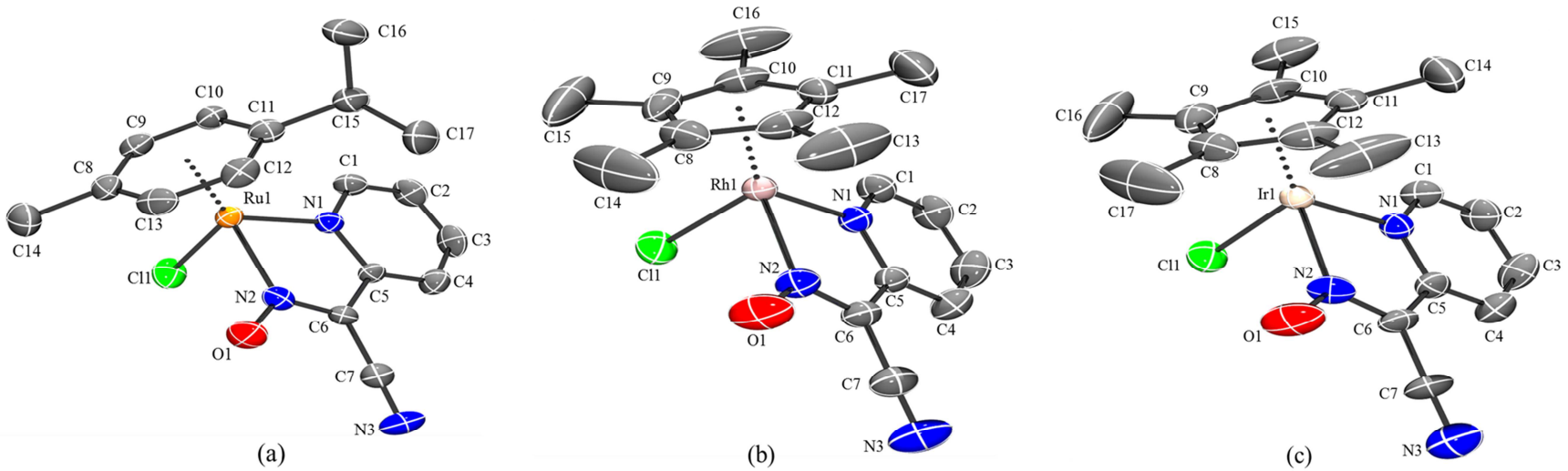

573

574 **Figure 1** (a) Ortep diagram of complex (**1**), (b) Ortep diagram of complex (**2**) and (c) Ortep diagram of complex (**3**) with 50%

575 probability thermal ellipsoids. Hydrogen atoms are omitted for clarity.

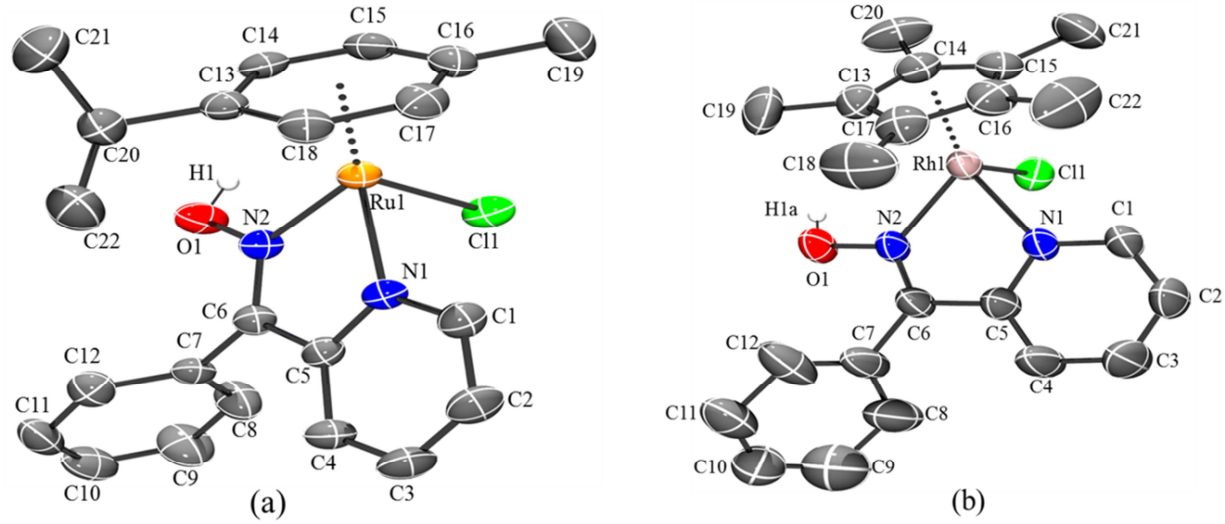

576

577 **Figure 2** (a) Ortep diagram of complex (**4**) and (b) Ortep diagram of complex (**5**) with 50%
578 probability thermal ellipsoids. Counter ions and hydrogen atoms (except on O1) are omitted for
579 clarity.

580

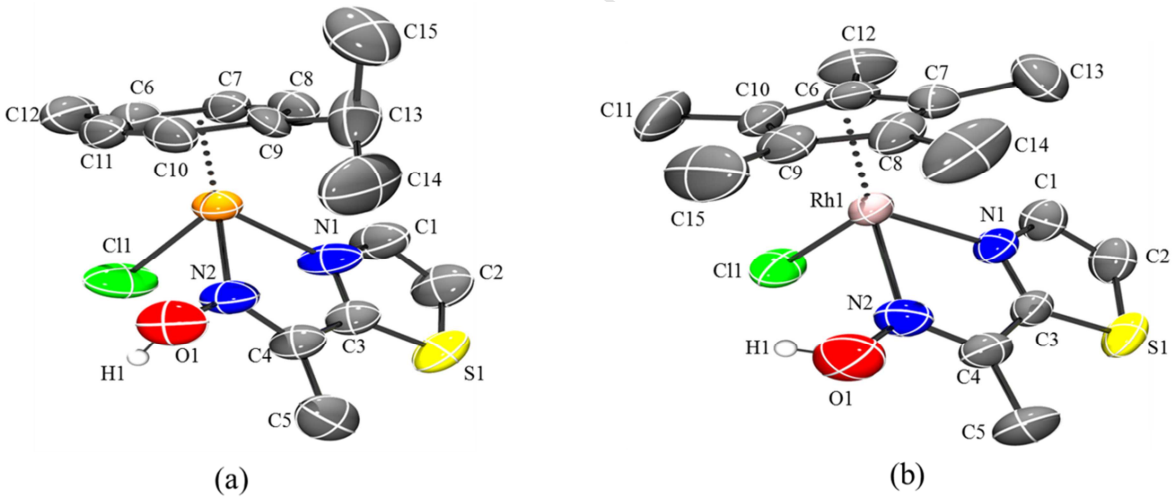

581

582 **Figure 3** (a) Ortep diagram of complex (**7**) and (b) Ortep diagram of complex (**8**) with 50%
583 probability thermal ellipsoids. Counter ions and hydrogen atoms (except on O1) are omitted for
584 clarity.

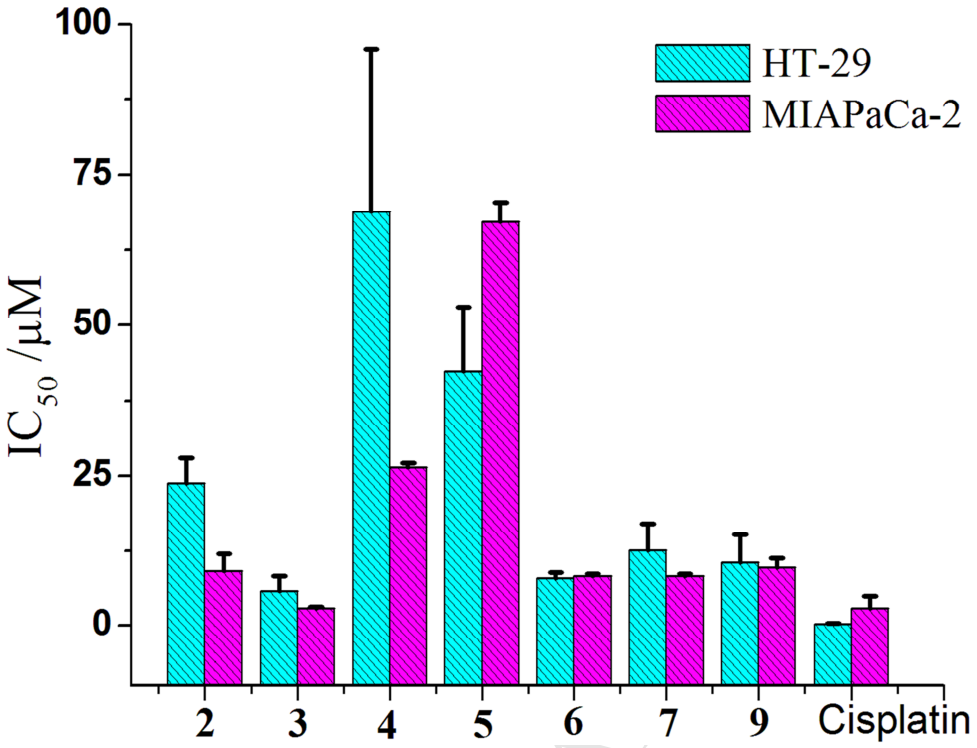

Figure 4 Response of HT-29 (human colorectal cancer) and MIAPaCa-2 (human pancreatic cancer) to compounds and cisplatin. Cell was exposed to compounds (**1**-**9**) for 96 hours. Each value represents the mean ± standard deviation from three independent experiments.

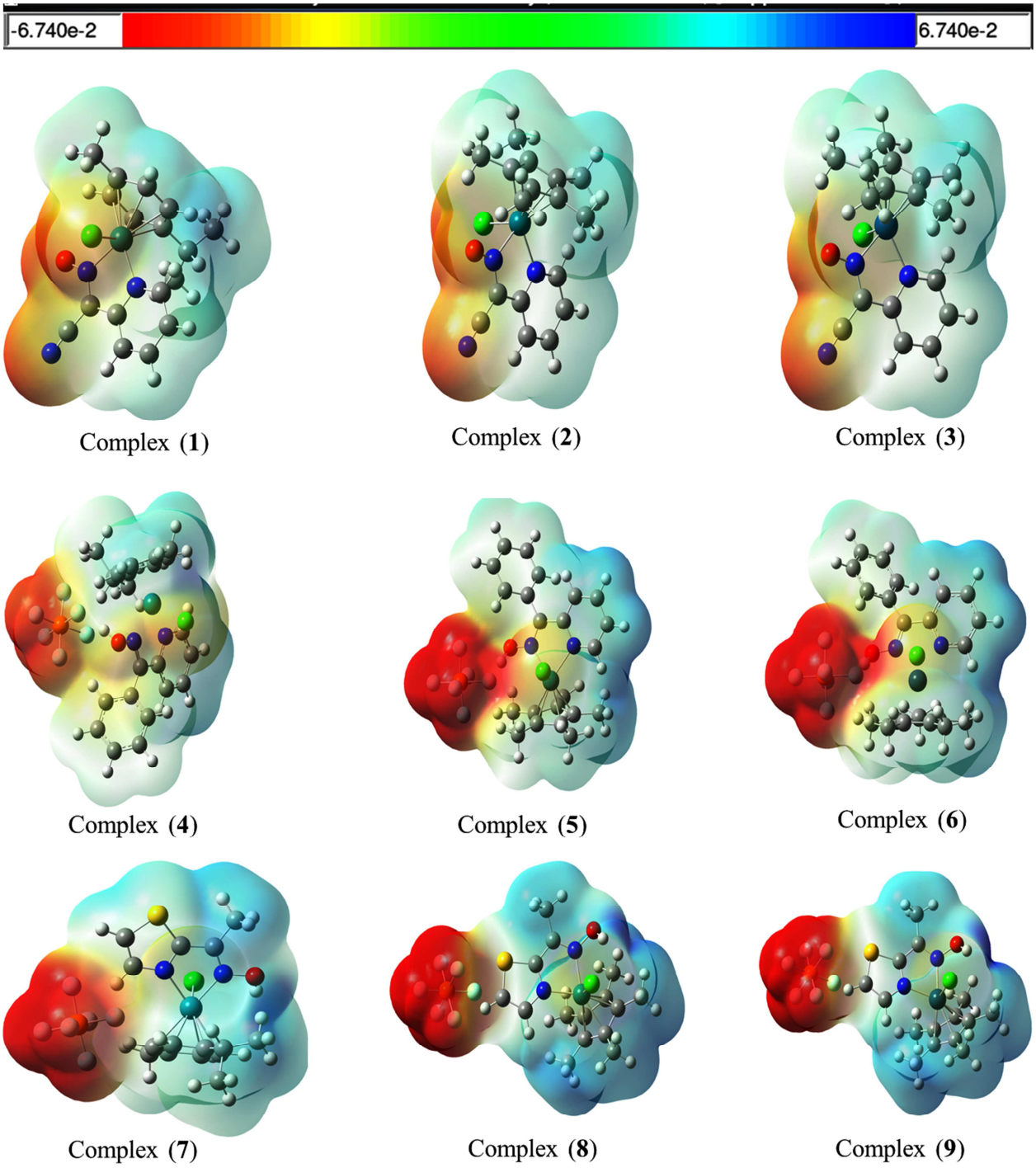

589

590 **Figure 5** Molecular electrostatic potential diagrams for complexes (**1**-**9**).

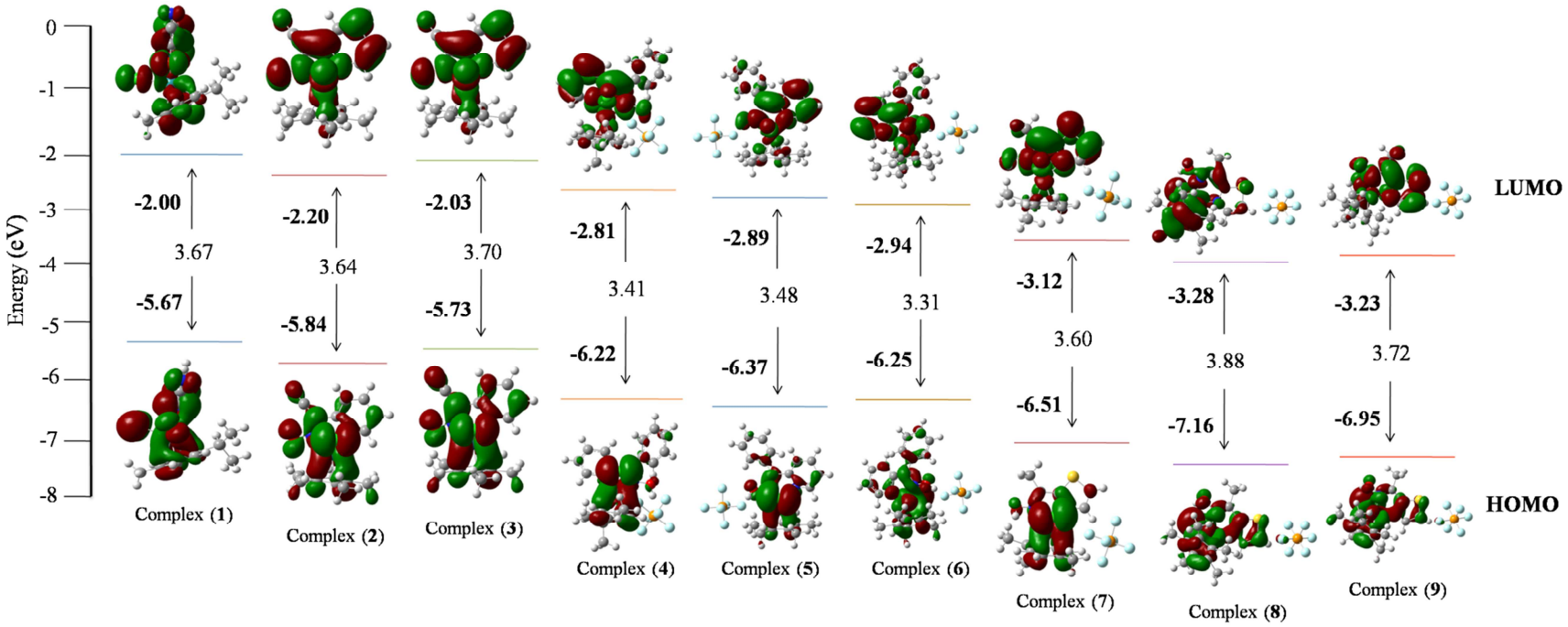

591

592 **Figure 6** HOMO, LUMO energies and their energy gaps of complexes (**1-9**).

Table 1 Crystal data and structure refinement parameters of complexes.

Compounds	[**1**]	[**2**]	[**3**]	[**4**]PF_6	[**5**]PF_6	[**7**]PF_6	[**8**]$PF_6{\cdot}H_2O$
Empirical formula	$C_{17}H_{18}ClN_3ORu$	$C_{17}H_{19}ClN_3ORh$	$C_{17}H_{19}ClN_3OIr$	$C_{22}H_{24}ClF_6N_2OPRu$	$C_{22}H_{25}ClF_6N_2OPRh$	$C_{15}H_{20}ClF_6N_2OPRuS$	$C_{15}H_{23}ClF_6N_2O_2PRhS$
Formula weight	416.86	419.71	509.00	613.92	616.77	557.88	578.74
Temperature (K)	292(2)	291(2)	295(2)	292(2)	296(2)	291(2)	295(2)
Wavelength (Å)	0.71073	0.71073	0.71073	0.71073	0.71073	0.71073	0.71073
Crystal system	Orthorhombic	Monoclinic	Monoclinic	Monoclinic	Triclinic	Monoclinic	Monoclinic
Space group	*Pca2₁*	*P2₁/c*	*P2₁/c*	*P2₁/n*	*P* $\bar{1}$	*P2₁/m*	*P2₁/c*
a (Å)/α (°)	14.9960(5)/90	8.3023(9)/90	8.3165(6)/90	9.0701(4)/90	9.0597(5)/67.455(5)	10.5576(7)/90	12.6553(5)/90
b (Å)/β (°)	7.8142(2)/90	27.612(2)/112.173(12)	27.5547(13)/112.388(7)	14.1127(6)/98.340(4)	12.7557(7)/82.956(5)	9.3658(7)/104.388(7)	10.8936(4)/98.858(4)
c (Å)/γ (°)	14.6872(4)/90	8.1421(8)/90	8.2007(5)/90	19.6319(9)/90	13.2635(8)/87.886(5)	13.2319(10)/90	16.3323(6)/90
Volume ($Å^3$)	1721.07(9)	1728.5(3)	1737.61(18)	2486.38(19)	1404.86(14)	1267.34(16)	2224.75(15)
Z	4	4	4	4	2	2	4
Density (calc) (Mg/m^{-3})	1.609	1.613	1.946	1.640	1.458	1.462	1.728
Absorption coefficient (μ) (mm^{-1})	1.073	1.149	7.844	0.865	0.815	0.919	1.117
F(000)	840	848	976	1232	620	556	1160
Crystal size (mm^3)	0.24 x 0.19 x 0.09	0.24 x 0.19 x 0.08	0.29 x 0.25 x 0.02	0.29 x 0.24 x 0.12	0.21 x 0.19 x 0.15	0.36 x 0.25 x 0.23	0.25 x 0.21 x 0.19
Theta range for data collection	3.05 to 28.74°	3.08 to 28.74°	3.03 to 28.73°	3.07 to 29.07°	3.22 to 29.12°	3.58 to 28.93°	3.14 to 29.01°
Index ranges	-20<=h<=16, -10<=k<=9, -17<=l<=18	-6<=h<=11, -36<=k<=36 -10<=l<=10	-11<=h<11, -30<=k<=36, -10<=l<=5	-10<=h<=12, -18<=k<=10, -26<=l<17	-11<=h<=11, -16<=k<=11, -17<=l<17	-12<=h<=14, -11<=k<=12, -10<=l<17	-13<=h<=15, -12<=k<=13, -22<=l<20
Reflections collected	6209	8785	9093	9847	9798	4790	8932
Independent reflections	3438 [R(int) = 0.0311]	3956 [R(int) = 0.0602]	3978 [R(int) = 0.0494]	5682 [R(int) = 0.0186]	6373 [R(int) = 0.0329]	3037 [R(int) = 0.0230]	5071 [R(int) = 0.0261]
Completeness to theta = 25.00°	99.7 %	99.5 %	99.6 %	99.6 %	99.5 %	98.3 %	99.5 %
Absorption correction	Semi-empirical from equivalents	Semi-empirical from equivalents	Semi-empirical from equivalents	Semi-empirical from equivalents	Semi-empirical from equivalents	Semi-empirical from equivalents	Semi-empirical from equivalents
Max. And min. transmission	0.9096 and 0.7828	0.9137 and 0.7700	0.8589 and 0.2094	0.9033 and 0.7875	0.8875 and 0.8474	0.8164 and 0.7331	0.8159 and 0.7677
Refinement method	Full-matrix least-squares on F^2	Full-matrix least-squares on F^2	Full-matrix least-squares on F^2	Full-matrix least-squares on F^2	Full-matrix least-squares on F^2	Full-matrix least-squares on F^2	Full-matrix least-squares on F^2
Data/restraints/parameters	3438/1/211	3956/0/213	3978/30/213	5682/0/311	6373/136/412	3037/172/229	5071/3/275
Goodness-of-fit on F^2	1.00	1.057	1.085	1.090	1.059	1.005	1.049
Final R indices [I>2sigma(I)]	R1 = 0.0322, wR2 = 0.0498	R1 = 0.0566, wR2 = 0.0966	R1 = 0.0526, wR2 = 0.1118	R1 = 0.0331, wR2 = 0.0728	R1 = 0.0473, wR2 = 0.1153	R1 = 0.0524, wR2 = 0.1426	R1 = 0.0475, wR2 = 0.1064
R indices (all data)	R1 = 0.0425, wR2 = 0.0526	R1 = 0.1081, wR2 = 0.1077	R1 = 0.0713, wR2 = 0.1217	R1 = 0.0426, wR2 = 0.0777	R1 = 0.0649, wR2 = 0.1241	R1 = 0.0640, wR2 = 0.1540	R1 = 0.0706, wR2 = 0.1211
Largest diff. peak and hole ($e.Å^{-3}$)	0.583 and -0.461	0.790 and -0.865	2.329 and -1.955	0.377 and -0.519	0.449 and -0.350	0.871 and -0.857	0.734 and -0.393
CCDC No.	1486252	1486253	1486254	1486255	1486256	1486257	1486258

Structures were refined on F_0^2: $wR_2 = [\Sigma[w(F_0^2 - F_c^2)^2] / \Sigma w(F_0^2)^2]^{1/2}$, where $w^{-1} = [\Sigma(F_0^2)+(aP)^2+bP]$ and $P = [\max(F_0^2, 0)+2F_c^2]/3$

595 Table 2 Selected bond lengths (Å) and bond angles (°) of complexes.

Complex	**1**	**2**	**3**	**4**	**5**	**7**	**8**
M(1)-CNT	1.696	1.799	1.803	1.696	1.788	1.728	1.775
M(1)-N(1)	2.073(3)	2.093(4)	2.084(7)	2.0587(18)	2.103(3)	2.09(2)	2.108(3)
M(1)-N(2)	2.028(3)	2.065(4)	2.039(7)	2.0854(19)	2.102(3)	2.08(3)	2.131(4)
M(1)-Cl(1)	2.3897(11)	2.3870(16)	2.391(2)	2.4191(7)	2.4225(10)	2.415(2)	2.3991(12)
M(1)-C_{ave}	2.203	2.165	2.170	2.205	2.157	2.179	2.149
N(2)-O(1)	1.271(4)	1.262(5)	1.254(9)	-----	----	----	----
N(2)-C(6)	1.330(5)	1.334(7)	1.360(11)	----	----	----	----
N(1)-M(1)-N(2)	77.81(13)	78.06(16)	78.0(3)	75.66(7)	74.92(11)	78.0(10)	75.16(15)
N(1)-M(1)-Cl(1)	85.22(9)	87.07(13)	84.8(2)	85.10(6)	87.58(9)	88.4(5)	88.51(10)
N(2)-M(1)-Cl(1)	84.87(9)	86.72(14)	85.6(2)	84.20(5)	89.30(9)	81.1(6)	89.14(11)
N(1)-M(1)-CNT	132.9	132.5	133.8	132.0	129.6	132.3	128.6
N(2)-M(1)-CNT	130.6	130.4	131.2	131.5	130.5	133.0	132.4
Cl(1)-M(1)-CNT	127.3	125.5	125.7	129.2	127.7	127.8	126.3

596 CNT represents the centroid of the arene/Cp* ring; C_{ave} represents the average bond distance of
597 the arene/Cp* ring carbon and metal atom.

598 Table 3 Response of HT-29 (human colorectal cancer) and MIAPaCa-2 (human pancreatic
599 cancer) to complexes (**1**-**9**) and cisplatin. Each value represents the mean ± standard deviation
600 from three independent experiments.

Complexes	IC_{50} (μM)	
	HT-29	MIAPaCa-2
1	>100	>100
2	23.74 ± 4.25	9.16 ± 2.89
3	5.82 ± 2.41	2.87 ± 0.26
4	68.83 ± 27.0	26.42 ± 0.67
5	42.32 ± 10.69	67.18 ± 3.16
6	7.92 ± 1.00	8.35 ± 0.29
7	12.56 ± 4.45	8.28 ± 0.42
8	>100	>100
9	10.54 ± 4.73	9.65 ± 1.68
Cisplatin	0.25 ± 0.11	2.84 ± 2.05

601 IC_{50} = concentration of the drug required to inhibit the growth of 50% of the cancer cells (μM).

602 Table 4 Energy gap, theoretical and experimental absorption bands, electronic transitions and
603 dominant excitation character for various singlet states of the complexes (**1**-**9**) calculated with
604 TD-DFT method.

The most important orbital excitations	Calculated λ (nm)	Energy gap E (eV)	Oscillator strength (f)	Dominant excitation Character	Experimental λ (nm)
			Complex **1**		
H→L	492.28	3.67	0.0021	L1→L1(ILCT)	
H-3→L	371.17	4.50	0.0025	L1→L1(ILCT)	370
H-1→L	362.01	3.93	0.0488	L1→L1(ILCT)	
H→L+3	304.45	4.61	0.1337	L1→L1(ILCT)	302
H→L+4	301.08	4.89	0.0161	L1→Cp*(LLCT)	
H-2→L+6	238.25	5.91	0.0034	Cl→L1(LLCT)	237
H-5→L+2	235.61	5.92	0.0485	Ru→L1(MLCT)	
			Complex **2**		
H→L	512.44	3.65	0.0046	L1→Rh(LMCT)	
H-2→L+2	364.41	4.59	0.0306	Cl→Rh(LMCT)	374
H→L+3	293.93	4.65	0.0438	L1→L1(ILCT)	289
H-6→L+1	253.61	5.77	0.1544	Rh→L1(MLCT)	255
			Complex **3**		
H→L	467.55	3.70	0.0036	L1→L1(ILCT)	
H-2→L	376.61	4.26	0.0523	Cl→L1(LLCT)	378
H-3→L+1	290.41	5.24	0.0192	L1→Ir(LMCT)	288
H-1→L+2	283.58	4.68	0.0903	L1→L1(ILCT)	
H-6→L+2	232.24	6.20	0.0153	Ir→L1(MLCT)	233
			Complex **4**		
H→L	452.56	3.42	0.0024	Ru→L2(MLCT)	
H-2→L	379.18	4.09	0.0245	L2→L2(ILCT)	376
H-1→L+2	357.48	4.46	0.0106	Ru→L2(MLCT)	
H-4→L+1	271.57	4.86	0.0021	L2→Ru(LMCT)	272
H-4→L+3	231.48	5.51	0.0180	L2→L2(ILCT)	233
			Complex **5**		
H→L	476.51	3.48	0.0093	Cl→L2(LLCT)	
H-1→L+2	357.91	4.27	0.1024	Cl→Ru(LMCT)	357
H-2→L	345.27	3.95	0.0105	Cl→L2(LLCT)	
H-6→L+1	267.72	5.28	0.0341	L2→Rh(LMCT)	266
			Complex **6**		
H→L	464.21	3.32	0.0223	Ir+Cl→L2(MLCT/ LLCT)	
H-1→L+1	352.62	4.52	0.0372	Cl→L2(LLCT)	360
H-7→L	294.49	5.07	0.0102	Ir→L2(MLCT)	296
H-3→L+1	290.68	5.13	0.0026	L2→L2(ILCT)	
			Complex **7**		
H→L	450.26	3.39	0.0038	L3→L3(ILCT)	

H-3→L	359.31	4.01	0.0091	Ru→L3(MLCT)	347
H-3→L+1	334.71	5.01	0.0036	Ru→L3(MLCT)	
H-4→L	293.24	5.59	0.0598	Ru→L3(MLCT)	297
H→L+3	291.42	5.30	0.0328	L3→Ru(LMCT)	
			Complex **8**		
H→L	484.85	3.87	0.0028	L3→L3(ILCT)	
H-1→L+2	345.81	4.52	0.0506	L3→L3(ILCT)	349
H-3→L	335.78	4.40	0.0238	Rh→L3(MLCT)	
H-3→L+2	285.07	4.73	0.0296	Rh→L3(MLCT)	287
H-8→L+1	229.87	5.27	0.0127	Rh→L3(MLCT)	
			Complex **9**		
H→L	463.13	3.72	0.0010	Ir→L3(MLCT)	
H-1→L+1	350.0	4.81	0.0182	Ir→L3(MLCT)	360
H-2→L	288.36	4.37	0.0250	L3→L3(ILCT)	

605

Highlights

- Neutral oximato and cationic oxime complexes of ruthenium, rhodium and iridium were isolated with electron withdrawing and electron donating substituted pyridyl oximes.
- DFT calculations demonstrate that the calculated values are in good agreement with the experimental data.
- Iridium based oximato and oxime complexes exhibited better activity than ruthenium and rhodium complexes.